AJAE

Open Access

Vol. 13, No. 3, pp. 196-211, September 2019
doi: https://doi.org/10.5572/ajae.2019.13.3.196
ISSN (Online) 2287-1160, ISSN (Print) 1976-6912

Research Article

Hygroscopic Behavior of Ammonium Sulfate, Ammonium Nitrate, and their Mixture Particles

Li Wu, Xue Li, Chul-Un Ro*

Department of Chemistry, Inha University, Incheon 22212, Republic of Korea

***Corresponding author.**
Tel: +82-32-860-7676
E-mail: curo@inha.ac.kr

Received: 2 September 2019
Revised: 9 September 2019
Accepted: 9 September 2019

ABSTRACT Inorganic species such as ammonium sulfate (AS) and ammonium nitrate (AN), which significantly affect air quality, visibility degradation, and climate change, occupy 20–50% among ambient fine aerosol mass. In the present study, laboratory generated, micrometer sized, pure AS, AN, and AS-AN mixture aerosol particles at 9 mixing ratios (mole fraction of AS, X_{AS} = 0.02, 0.035, 0.1, 0.15, 0.2, 0.28, 0.5, 0.6, and 0.8) were examined systematically to observe their hygroscopic behavior, to derive experimental phase diagrams for efflorescence and deliquescence, and to obtain chemical micro-structures using in-situ Raman microspectrometry (RMS). All the nebulized AS-AN mixture particles experienced only one-stage efflorescence at 15–40% relative humidity (RH) during dehydration process, revealing that all the compounds in the particles crystallized nearly simultaneously. Nebulized AS-AN mixture particles of eutonic composition (X_{AS} = 0.035) showed single-stage transition at a mutual deliquescence relative humidity (MDRH) of 63.6%, whereas the others exhibited two-stage deliquescence transitions during humidification process, i.e., the eutonic component dissolved at MDRH, and the remainder in the solid phase dissolved completely at their DRHs, resulting in a phase diagram composed of four different phases, as predicted thermodynamically. The measured MDRH and second DRHs of mixture particles with mixing ratios of $0.035 < X_{AS} < 0.33$ are either higher or lower than the theoretical values, while only the experimental second DRHs of mixture particles with mixing ratios of $X_{AS} > 0.33$ are higher than the theoretical values calculated from E-AIM model, which might be due to the variations of crystal formation when the efflorescence occurred. As reported previously, AS and AN mixture droplets can crystallize as the mixture of pure crystal and stable and/or metastable double salts (2AN·AS and/or 3AN·AS, respectively) and the degree of metastability might differ under different conditions. Our results also indicate that the AS-AN mixture particles can crystallize into different forms, leading to diverse MDRHs and DRHs than the theoretical ones, which can promote their capability of probable heterogeneous chemistry on the aqueous aerosol surface.

KEY WORDS Ammonium sulfate (AS), Ammonium nitrate (AN), Mixture, Hygroscopicity, In-situ Raman microspectrometry (RMS)

1. INTRODUCTION

Ammonium sulfate (AS) and ammonium nitrate (AN) particles, which can exist internally mixed in the polluted air, occupy a major portion of ambient fine aerosol mass and their levels increase with the elevated $PM_{2.5}$ levels during haze events (Sun

et al., 2019; Sun *et al.*, 2018; Huang *et al.*, 2014; Lightstone *et al.*, 2000; Zhang *et al.*, 2000). The internal mixture of AS and AN particles were reported to exist as the mixtures of pure AS and AN and double salts (3AN·AS and 2AN·AS), based on the studies of thermodynamic models (Clegg *et al.*, 1998), laboratory generated aerosols (Wang *et al.*, 2011; Ling and Chan, 2007), and real ambient aerosol particles using a non-destructive Raman analysis (Sun *et al.*, 2019). Many studies were also conducted for analyzing the mixture of AS and AN with organic acids as they dominate the fine aerosol mass (Wu *et al.*, 2019; Kim *et al.*, 2018) and may alter their properties mutually (Wang *et al.*, 2018; Schroeder and Beyer, 2016; Wang *et al.*, 2016; Zawadowicz *et al.*, 2015; Meyer *et al.*, 2009). The previous study showed that the secondary formation of AS and AN from SO_2, NO_2, and NH_3 on wet aerosols facilitated the haze formation in China (Sun *et al.*, 2018), where the sulfate and nitrate formation rates were, in turn, promoted by heterogeneous reactions on the liquid surface of haze aerosols (Cheng *et al.*, 2016). It was reported that the heterogenous chemical reactions on the surface of aerosol particles are much faster in aqueous phase (Hallquist *et al.*, 2003). The ability of the aerosol particles to uptake water in the air is dependent on one of the most important physicochemical properties, i.e., the hygroscopicity (Jing *et al.*, 2016). Therefore, studies on the hygroscopicity of AS and AN particles are important to comprehensively understand their behavior when interacting with water vapor and further their impacts on the heterogeneous chemical reactions, atmospheric environment, and human health.

The importance of understanding the hygroscopic behavior of inorganic aerosol particles has been well described previously (Gupta *et al.*, 2015a, b). The study on the hygroscopic properties of inorganic salt particles can provide important insights into (i) alteration of the particle aerodynamic properties, (ii) cloud-droplet nucleation efficiency, (iii) optical properties that contribute to the direct and indirect radiative forcing on climate change, and (iv) the possible physicochemical changes that the aerosols undergo through complex heterogeneous chemical reactions with atmospheric gas-phase species (Leng *et al.*, 2016; Liu *et al.*, 2008; Wang and Martin, 2007; Krueger *et al.*, 2003; Haywood and Boucher, 2000; ten Brink, 1998; Potukuchi and Wexler, 1995). Up until now, a few studies either on deliquescence or efflorescence behavior of mixed AS-AN particles have been performed. Chan *et al.* (1992) measured the water activities for mixed AS-AN droplets using an Electro Dynamic Balance (EDB) apparatus and their data were mostly consistent with model predictions. The deliquescence behavior of AS-AN mixtures with mixing ratios of 1:1 and 1:5 was examined and it was reported the mixture of 1:5 behaved like pure AN particles due to the lack of deliquescence and crystallization (Ten Brink and Veefkind, 1995). Ge *et al.* (1998) also investigated the deliquescence behavior of mixed AS-AN particles with AS mole fractions (X_{AS}) of 0.02, 0.06, 0.2, 0.28, 0.5 and 0.8 using rapid single-particle mass spectrometry (RSMS), where no exact deliquescence relative humidity (DRH) and mutual DRH (MDRH) were reported and they claimed that the experimental deliquescence behavior of AS-AN mixtures was very complicated and not consistent with thermodynamic predictions, probably due to the low crystallization point of AN. The 1:1 AS-AN mixture particles were examined using EDB/Raman system and MDRH, DRH, and efflorescence RH (ERH) were reported (Lee *et al.*, 2008). Crystallization of AS-AN particles of three mixing ratios (X_{AS} = 0.5, 0.6, and 0.82) were examined by aerosol flow tube infrared spectroscopy (Schlenker *et al.*, 2004; Martin *et al.*, 2003). AS and AN mixtures of X_{AS} = 0.1–0.9 were determined theoretically and experimentally, however, the molecular structure and composition changes were not available (Sun *et al.*, 2018). The hygroscopic behavior of AS and AN mixture particle are still under no comprehensive understanding. Full phase diagrams, covering the entire range of mixing ratios, are needed to fully understand the hygroscopic behavior of multi-component aerosol particles (Martin, 2000).

In the present study, the hygroscopic behavior, physical states/phases, and micro-structures of the laboratory-generated, micrometer-sized, pure AS, AN, and mixture particles (covering 9 mixing ratios with X_{AS} = 0.02–0.8) were examined systematically at room temperature by in situ Raman microspectrometry (RMS). The phase transitions were observed by monitoring the size change of the particles as a function of RH. And RMS can provide aerosol compositions, molecular interactions, and particle phase states sensitively for better understanding of the hygroscopic behavior of complex aerosol particles (Li *et al.*, 2017; Wang *et al.*, 2017; Lee *et al.*, 2008). The experimentally measured MDRHs and DRHs were compared with those derived theoretically from the Extended Atmospheric Inorganics Model (E-AIM) calculations.

2. EXPERIMENTAL SECTION

2.1 Preparation of Mixed AS-AN Particles

Pure solutions (0.5 M each) of AS and AN (AS > 99.9% purity, Aldrich; AN > 99.9% purity, Aldrich) were prepared, and the AS-AN mixture solutions were made by mixing the two pure ones volumetrically. The mixed AS-AN droplets were deposited by nebulizing the aqueous solutions on Si wafer substrates (MTI Corporation, 99.999% purity) using a single jet atomizer (HCT4810). The size of the droplets ranged from 1–15 μm. The pure AS particles were dry deposited on the Si wafer substrates for hygroscopic measurement to check the accuracy of the experimental setup (Chan and Chan, 2005).

The AS-AN mixture particles with 9 different mixing ratios were investigated in this study, i.e., 8 compositions with the AS mole fractions of 0.02–0.8 (X_{AS} = 0.02, 0.1, 0.15, 0.2, 0.28, 0.5, 0.6, and 0.8, where X_{AS} represents the mole fraction of AS) and an eutonic composition (X_{AS} = 0.035, which was calculated from the ionic activity products predicted by the Extended Atmospheric Inorganics Model (E-AIM)). The AS-AN mixture system has an AN-dominant eutonic composition and, hereafter, particles with a composition of $X_{AS} > 0.035$ were notated as AS-rich and those with $X_{AS} < 0.035$ were as AN-rich, in the context of thermodynamics.

2.2 Hygroscopic Property Measurement

In situ RMS measurements were performed under controlled RHs to observe the hygroscopic behavior, structural changes, and chemical compositional variations of the aerosols generated from the AS-AN solutions. The apparatus consists of three parts: (A) see-through impactor, (B) Raman microscope/spectrometer, and (C) humidity controlling system. The Si wafer substrate was mounted on the impaction plate in the see-through impactor. A more detailed discussion of the impactor and humidity controlling system can be found elsewhere (Li *et al.*, 2017; Gupta *et al.*, 2015a; Ahn *et al.*, 2010). Briefly, the RH inside the impactor was controlled by mixing dry and wet (saturated with water vapor) N_2 gases. The flow rates of the dry and wet N_2 gases were controlled by two mass flow controllers to obtain the desired RH in the range of ~1–95%, which was monitored by a digital hygrometer (Testo 645). The digital hygrometer was calibrated using a dew-point hygrometer (M2 Plus-RH, GE), providing RH readings with ±0.5% reproducibility. All hygroscopic experiments were conducted at room temperature (T = 22 ± 1°C). The in-situ Raman spectra and optical images of the aerosol particles deposited on the Si wafer substrate were recorded by Labspec6 using a confocal Raman microspectrometer (XploRA, Horiba Jobin Yvon) equipped with a 50×/0.5 numerical aperture objective (Olympus). An excitation laser with a wavelength of 532 nm and 6 mW power was used and the scattered Raman signals were detected at specific RHs during hygroscopic measurement using an air-cooled multichannel charge-coupled device (CCD) detector. The data acquisition time was 90 s for each measurement and the spectral resolution was 1.7 cm^{-1} using 1800 gr/mm. The signal from Si wafer was subtracted from the spectra for clearance. The optical images were recorded continuously in steps of 1% with the size of 904 × 690 pixels during firstly dehydration (by decreasing RH from ~95 to ~1%) and then humidification (by increasing RH from ~1 to ~95%) experiments using a video camera assembled in the Raman instrument and were processed using image analysis software (Matrox, Inspector v9.0). The changes in particle size with the variation of RH were monitored by measuring the particle 2-D area in the optical images to generate the hygroscopic curves (Ahn *et al.*, 2010).

3. RESULTS AND DISCUSSION

3.1 Hygroscopic Behavior of Pure AS and AN Particles

The dehydration and humidification curves shown in Fig. 1 are represented as the area ratio (A/A_0: left-hand axis), where the 2-D projected particle area at a given RH (A) is divided by that before starting the humidification process (A_0). Aerosol particles generated from a pure AS solution showed typical hysteresis curves with ERH = 43.2–37.6% and DRH = 80.7 (±0.2)%, which are consistent with the reported ones (Wang *et al.*, 2017; Liu *et al.*, 2016; Laskina *et al.*, 2015; Denjean *et al.*, 2014; Krieger *et al.*, 2012; Adachi *et al.*, 2011; Ciobanu *et al.*, 2010; Martin *et al.*, 2003). The optical images and the Raman spectra in Fig. 1 show the distinct particle morphology change, the red shift of the SO_4^{2-} peak from 977 to 972 cm^{-1}, and the decrease of the FWHH (full width at half height) of SO_4^{2-} peak at RH = 41.3% during dehydration process, indicating the efflorescence of the AS particle (Yeung and Chan, 2010). During the humidification process, the particle maintained the structure until RH = 77.1% where the particle size started to decrease due to

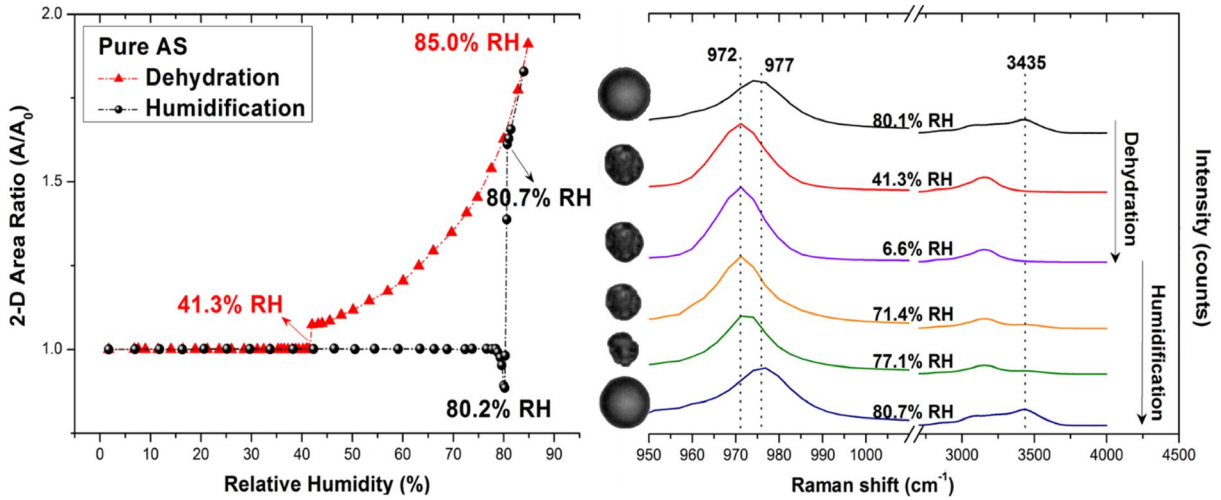

Fig. 1. Hygroscopic curve, corresponding optical images, and Raman spectra at specific RHs of a pure AS particle. The recorded transition RHs during the dehydration and humidification processes are marked with arrows in the hygroscopic curve.

the structural re-arrangements by the absorption of moisture on the lattice imperfections (Gysel *et al.*, 2002) until RH = 80.2%, after which the particle size increased sharply, the SO_4^{2-} peak shifted back to 977 cm^{-1}, and the FWHH became wider when the particle dissolved at RH = 80.7%. The Raman peak of water at 3435 cm^{-1} can be clearly distinguished between aqueous and dry phases. These DRH and ERH of the single-component AS aerosol particles are denoted as those of the "pure AS limit".

The wet-deposited AN particles exhibited two types of hygroscopic behavior as shown in Fig. 2. Type 1 particles showed the typical hysteresis hygroscopic curves with definite phase transitions at ERH = 23.9–13.7% and DRH = 64.6 (±0.3)%, which are similar to the values reported previously (Yeung and Chan, 2010; Chang and Lee, 2002; Tang, 1996; Chan *et al.*, 1992). Hereafter, the DRH of the "pure AN limit" is defined as RH = 64.6%. While type 2 particles shrank and grew continuously without any phase transition during the dehydration and humidification processes, which has also been observed before (Sun *et al.*, 2018; Hu *et al.*, 2011; Yeung and Chan, 2010; Liu *et al.*, 2008; Cziczo and Abbatt, 2000; Dougle *et al.*, 1998). The different behavior of the AN particles is attributed to the different nucleation mechanisms, i.e. homogeneous and heterogeneous nucleations, for pure and impure (seed-containing) AN particles, respectively (Lightstone *et al.*, 2000). Similar situation was reported for $NaNO_3$ and NH_4HSO_4 particles (Jing *et al.*, 2018; Kim *et al.*, 2012; Gibson *et al.*, 2006; Hoffman *et al.*, 2004). Fig. 2 also shows the corresponding optical images and Raman spectra for two types of the AN particles. The red shift of the NO_3^- peak from 1045 to 1039 cm^{-1} with the decrease of FWHH and the distinct morphology change of the type 1 particle at RH = 18.8% indicate the efflorescence, while the type 2 particle maintained the peak pattern and position of the Raman spectra and circular morphology only with the size changes when the RH was down to RH = 1.5%, even though the Raman peak of water at 3484 cm^{-1} became undetectable. The nebulized AN particle may exist as supersaturated particles with no visible ERHs. A previous study also showed that AN particles exist as anhydrous liquid-like or amorphous state and the crystallization of them can be promoted by AS instead of soot (Dougle *et al.*, 1998).

3.2 Hygroscopic Behavior of Mixed AS-AN Particles

Stepwise efflorescence and deliquescence transitions generally happen for two-component inorganic hygroscopic salt particles and theoretical aspects of the hygroscopic properties of binary mixture particles were discussed in detail elsewhere (Gupta *et al.*, 2015b; Li *et al.*, 2014). During the dehydration process, a component of the aqueous droplets precipitates first at their specific ERH depending on their mixing ratio and the second crystallization from the remnant eutonic solution occurs at a mutual ERH (MERH) with further decrease in RH, which is independent of the mixing ratios, forming a heterogeneous, core-shell crystal structure owing to the two-stage crystallization process (Ge *et al.*, 1996). Similarly, during the humidification process, it has been predicted

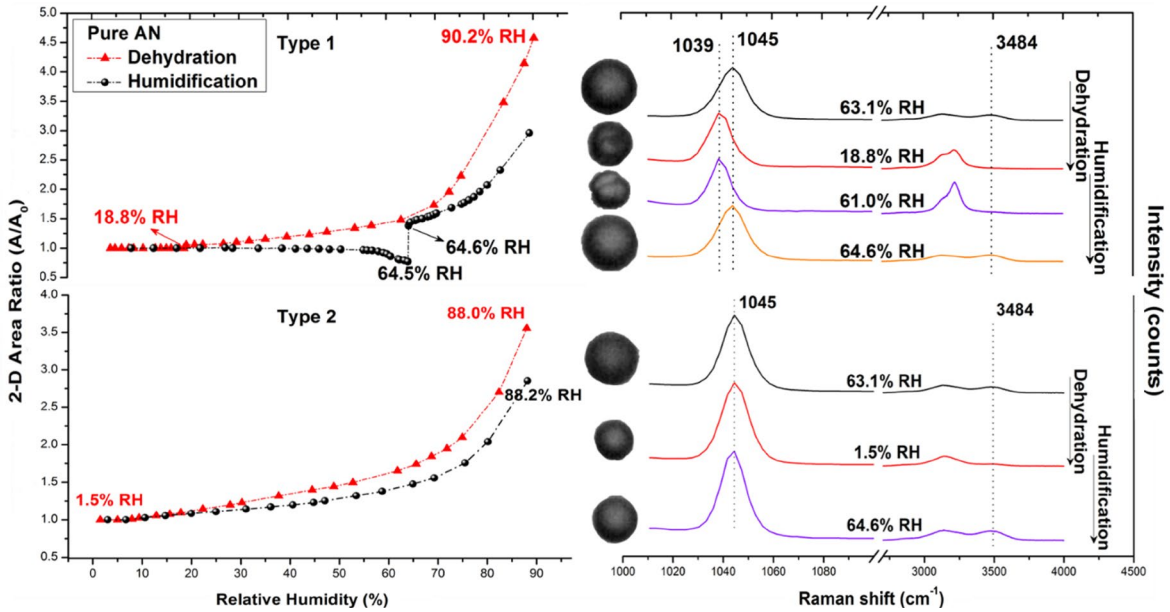

Fig. 2. Hygroscopic curve, corresponding optical images, and Raman spectra at specific RHs of two types of pure AN particles. The recorded transition RHs during the dehydration and humidification processes are marked with arrows in the hygroscopic curve.

that an aqueous phase with a eutonic composition is formed first at MDRH, which is independent of the mixing ratios; and the remnant solids in the core dissolve later at their second DRH, which depends on the mixing ratios (Wexler and Seinfeld, 1991). Efflorescence is a kinetic or rate-driven process that requires a sufficient activation energy to overcome a kinetic barrier which depends on many factors such as mixing states of chemical components, micro-physical states, supersaturation levels, vapor pressure, interfacial tension, viscosity, inter-ionic forces, and solute-water and solute-solute interactions, so that no general theoretical model that covers the efflorescence of single or multi-component aerosol particles is available (Martin, 2000; Cohen *et al.*, 1987). As it was also reported that the physical states (i.e., amorphous or crystalline and hydrated or anhydrous nature) of salts play a vital role in water absorption, diffusion, uptake or dissolution, evaporation, solidification, and morphology changes during the humidification and dehydration processes (Mikhailov *et al.*, 2009), the best way to understand the efflorescence behavior of aerosols is through experimental measurements (Seinfeld and Pandis, 2006). Deliquescence is a thermodynamic process that can be described by thermodynamic considerations (Krieger *et al.*, 2012). Thermodynamic models, such as the Extended Atmospheric Inorganics Model (E-AIM) (http://www.aim.env.uea.ac.uk/aim/aim.php) (Wexler and Clegg, 2002; Ansari and Pandis, 1999; Tang, 1976), can be used to predict the MDRHs and second DRHs.

Hygroscopic behavior was investigated on 20–50 particles of each mixing ratio in this work. The mixture particles could be divided into three categories: (i) $X_{AS}=0.035$ (the eutonic composition), (ii) AN-rich ($X_{AS}=0.02$), and (iii) AS-rich ($X_{AS}>0.035$), which are discussed in the following sections.

3.2.1 Eutonic Particles ($X_{AS}=0.035$)

Fig. 3 shows the 2-D projected area ratio plot as a function of RH obtained during the dehydration and humidification processes for a representative eutonic particle. During the dehydration process, the particle decreased gradually in size due to water evaporation until a single-phase transition from the liquid droplet to the solid particle was observed at RH = 24.8–24.5%, after which, the size of the particle kept consistent with the further decrease in RH. All the eutonic droplets showed ERH in the range of RH = 27.4–20.5%. During the humidification process, a single-phase transition from the solid particle to the liquid droplet was observed at RH = 63.1–63.6%, after which, the size of the liquid droplet grew gradually and continuously with the further increase in RH. As the eutonic particles deliquesced at RH = 63.6 (±0.5)%, the DRH approached the MDRH of the mixed AS-AN particles.

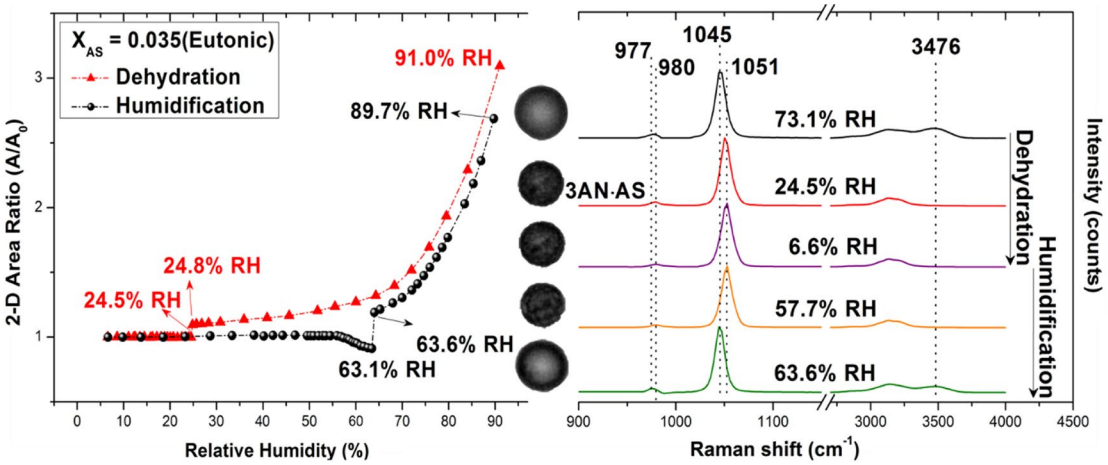

Fig. 3. Hygroscopic curve, corresponding optical images, and Raman spectra at specific RHs of a particle with the eutonic composition (X_{AS} = 0.035). The recorded transition RHs during the dehydration and humidification processes are marked with arrows in the hygroscopic curve.

To clearly assess the compositional and structural changes during hygroscopic processes, Raman spectra and corresponding optical images of the particle recorded at specific RHs were also shown in Fig. 3, where SO_4^{2-} and NO_3^- Raman peaks are at 977 and 1045 cm^{-1} at RH = 73.1% during the dehydration process, respectively, indicating that the aerosol is in the droplet form as also suggested by the water peak at 3476 cm^{-1} and the round-shape with smooth surface in the optical image. At RH = 24.5% during dehydration process, the rough-surfaced particle in the optical image and the disappearance of the water peak in the Raman spectrum confirmed the crystallization of the particle. And the two Raman peaks shifted rightward to 980 and 1051 cm^{-1}, respectively, indicating the eutonic mixture droplet crystallized into the metastable double salt 3AN·AS based on the previous study (Sun *et al.*, 2019; Wang *et al.*, 2011; Ling and Chan, 2007). The particle maintained the structure and composition until RH = 55.8% and decreased a little in size until RH = 63.1%, which are supported by the optical image and Raman spectrum at RH = 57.7%, and dissolved again to become the mixture of AS-AN droplet at RH = 63.6% during humidification process with the SO_4^{2-} and NO_3^- peaks shifting back to 977 and 1045 cm^{-1}, respectively.

3.2.2 AN-rich Particles (X_{AS} = 0.02)

Hygroscopic behavior of X_{AS} = 0.02 was conducted as an example of AN-rich particles. Fig. 4 shows the 2-D projected area ratio plot as a function of RH obtained during the dehydration and humidification processes, the optical images, and the corresponding Raman spectra at the transition points of the representative AN-rich particle of X_{AS} = 0.02. During the dehydration process, the liquid droplet gradually decreased in size with decreasing RH and showed a phase transition at RH = 15.1–14.4%. As shown in the optical images and Raman spectra in Fig. 4, the droplet with the NO_3^- peak at 1045 cm^{-1} at RH = 62.5% (SO_4^{2-} peak is too small to be shown here due to its low content), decreased in size abruptly at RH = 14.4%, forming a solid particle, which is clearly seen by its rough surface, with the NO_3^- peak shifting to 1051 cm^{-1} and becoming asymmetric, indicating the droplet effloresced into the metastable double salt 3AN·AS (Sun *et al.*, 2019; Wang *et al.*, 2011; Ling and Chan, 2007). The particle maintained the phase and structure with the further decrease in RH.

During the humidification process, the size and shape of the particles remained constant until a slight decrease in size was observed at RH = 53.5–62.8%, which is also suggested by the optical image of the particle at RH = 58.9%. All the particles absorbed water and showed a first partial deliquescence transition at RH = 63.6%, which is the DRH of the eutonic composition, i.e., MDRH of the AS-AN system. And the particle became a liquid eutonic shell with a solid core structure, which is reported as a solid-aqueous equilibrium state (Sun *et al.*, 2018) as shown in the optical image of the particle at RH = 63.6%. Raman spectrum of the particle center at RH = 63.6% indicates the solid core is pure AN crystal. Upon the fur-

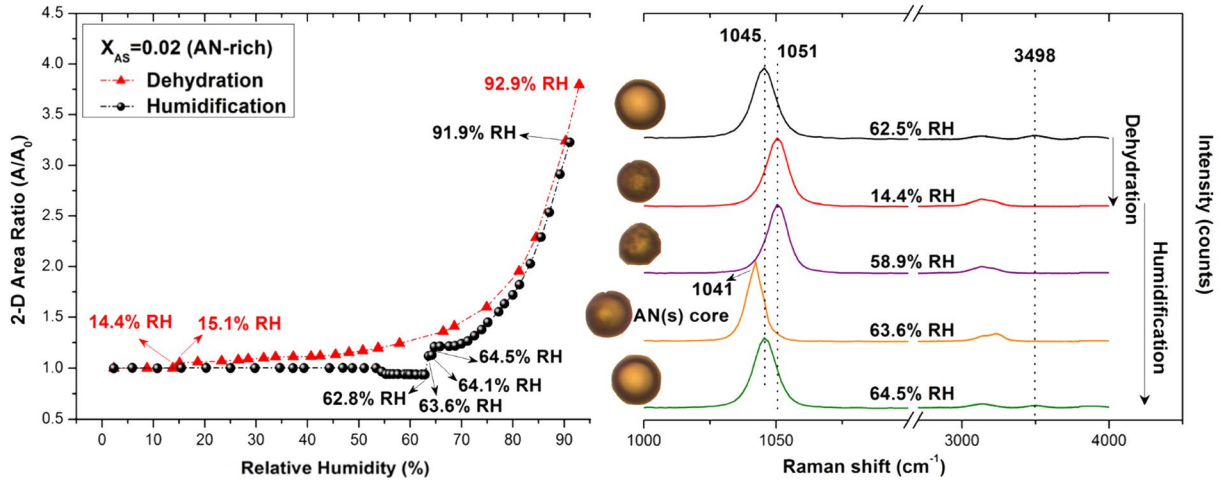

Fig. 4. Hygroscopic curve, corresponding optical images, and Raman spectra at specific RHs of an AN-rich particle ($X_{AS}=0.02$). The recorded transition RHs during the dehydration and humidification processes are marked with arrows in the hygroscopic curve.

ther increase in RH, the particles absorbed water and deliquesced at RH = 64.5%, i.e., second DRH, where the AN solid core dissolved completely. The particle grew continuously thereafter with the further increase in RH.

Most particles crystalized in the RH range of 19.3–13.3% and deliquesced firstly at MDRH = 63.6% and then at second DRH = 64.5%. However, 4 out of 43 particles in the image field shrank and grew continuously in size without any phase changes, showing similar behavior to that of the pure AN particles, and the non-crystallization would be due to the lack of good heterogeneous nuclei that can promote the crystallization as reported previously (Ge *et al.*, 1998). The phase of AN in dry particles can notably affect the hygroscopicity of mixtures (Liu *et al.*, 2016).

3.2.3 AS-rich Particles ($X_{AS}>0.035$)

Based on the deliquescence phase diagram (which will be explained in section 3.4), AS-rich particles are divided into 2 parts: $0.035<X_{AS}<0.33$ and $X_{AS}>0.33$.

3.2.3.1 AS-rich Particles of $0.035<X_{AS}<0.33$

Fig. 5 presents the 2-D area ratio plot as a function of RH of an AS-rich particle ($X_{AS}=0.1$). The liquid droplet at RH = 90.9% gradually decreased in size with decreasing RH and effloresced at RH = 21.9% with the particle shape becoming irregular in the optical image, the water peak at 3460 cm^{-1} disappearing, and the SO_4^{2-} and NO_3^- peaks shifting from 977 and 1045 to 975 and 1047 cm^{-1}, respectively, in the Raman spectra during dehydration process. The Raman spectra of the crystal do not resemble any characteristic one either for the AS crystal or the double salts (3AN·AS and/or 2AN·AS), indicating the possible formation of a crystal in an intermediate or mixing phase of the crystals. All the droplets showed ERH in the range of RH = 25.8–19.0%. During the humidification process, the particle remained consistent until RH = 52.2%, then decreased in size until RH = 61.9%, and experienced first deliquescence at RH = 62.3%, which differed from the MDRH = 63.6 (±0.3)% of the eutonic composition ($X_{AS}=0.035$), confirming that the mixture droplet did not crystallize into the same eutonic composition when efflorescence occurred. And the Raman spectra at RH = 62.3% did not show much difference compared with that of the crystal. This may be because the Raman signal of the aqueous eutonic composition formed under this mixing ratio is hindered by the remnant crystal showing the Raman peak at low wavenumber, and the eutonic composition is not very hygroscopic to promote detectable Raman peak of water at high wavenumber. With the further increase in RH, the particle absorbed water continuously and dissolved at RH = 65.8%. The optical image showed the droplet morphology and the SO_4^{2-} and NO_3^- peaks shifted back to 977 and 1045 cm^{-1}, respectively, in Raman spectrum of the particle. The behavior of the AS-rich particle of $X_{AS}=0.15$ is similar as that of $X_{AS}=0.1$, with the ERH in the range of 27.8–19.2%, the MDRH of 62.5 (±0.4)%, and DRH of 66.4 (±0.3)%.

Fig. 6 presents the 2-D area ratio plot as a function of

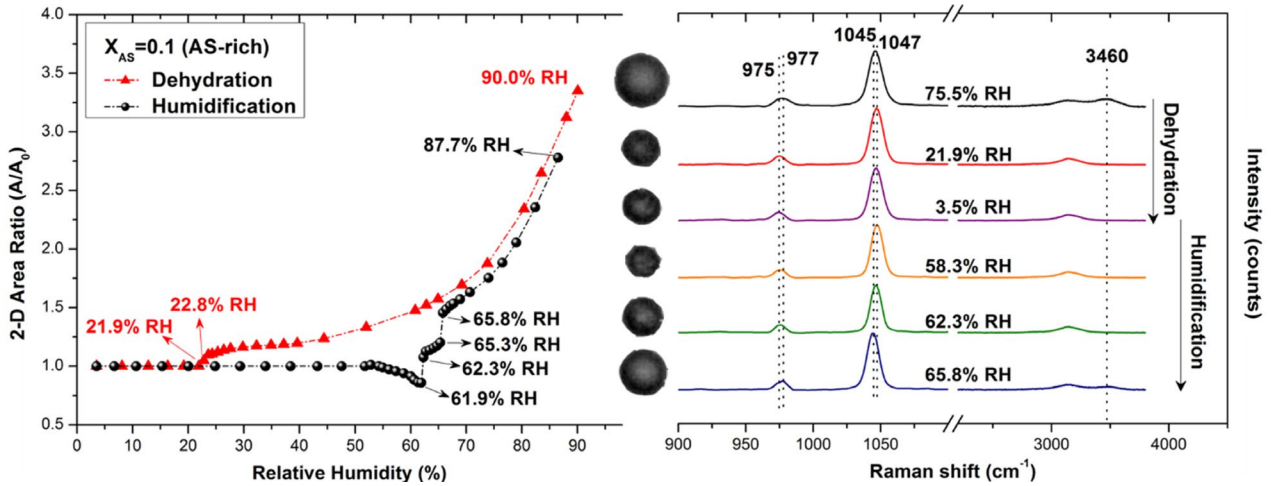

Fig. 5. Hygroscopic curve, corresponding optical images, and Raman spectra at specific RHs of an AS-rich particle ($X_{AS}=0.1$). The recorded transition RHs during the dehydration and humidification processes are marked with arrows in the hygroscopic curve.

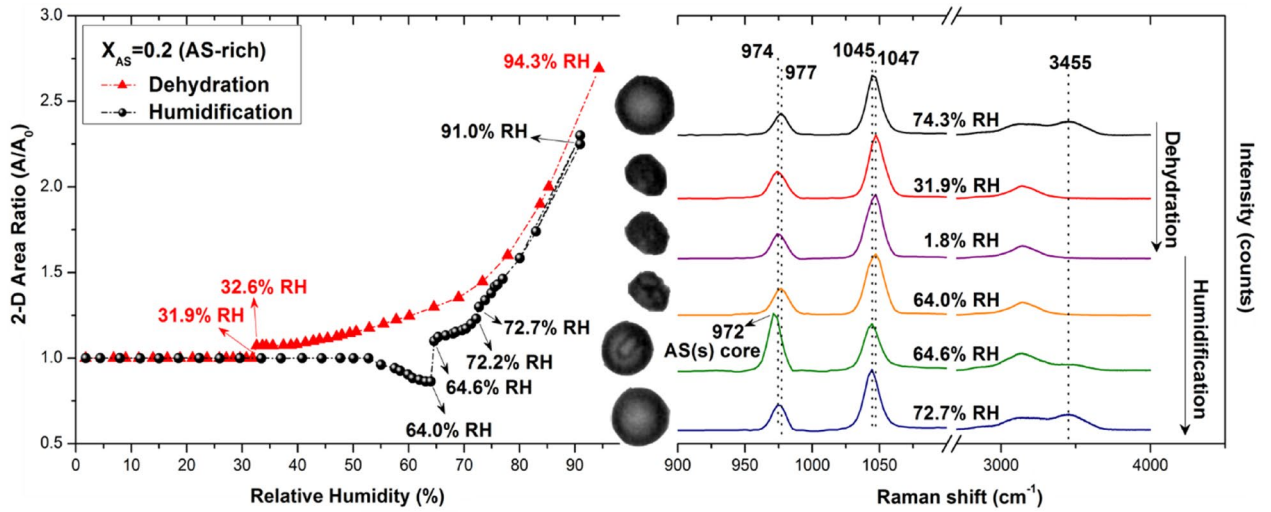

Fig. 6. Hygroscopic curve, corresponding optical images, and Raman spectra at specific RHs of an AS-rich particle ($X_{AS}=0.2$). The recorded transition RHs during the dehydration and humidification processes are marked with arrows in the hygroscopic curve.

RH of another AS-rich particle ($X_{AS}=0.2$). The particle behaved similarly with the particles of $X_{AS}=0.1$ during the dehydration process. All the droplets showed ERH in the range of 32.1–22.3%. During the humidification process, the particle maintained the structure until RH = 52.5%, experienced the decrease in size until RH = 64%, and deliquesced firstly at RH = 64.6%, which differed from the MDRH = 63.6 (±0.3)% of the eutonic composition and that of the $X_{AS}=0.1$ and 0.15 (62.3 (±0.5)% and 62.5 (±0.4)%, respectively). The optical images of the particle showed an obvious solid core inside the eutonic droplet which is the pure AS, indicated by the Raman spectra with the SO_4^{2-} peak at 972 cm^{-1}. The AS solid core dissolved at the second DRH of 72.7%. The optical image showed the droplet morphology and the SO_4^{2-} and NO_3^- peaks shifted back to 977 and 1045 cm^{-1}, respectively, in Raman spectrum of the particle.

The AS-rich particles of $X_{AS}=0.28$ show the similar behavior to that of $X_{AS}>0.33$, which is not separately shown here.

3.2.3.2 AS-rich Particles of $X_{AS}>0.33$

As for the particles of $X_{AS}>0.33$, Fig. 7 presents the 2-D area ratio plot as a function of RH, optical images,

and corresponding Raman spectra at the transition points only for an $X_{AS}=0.6$ particle as an example, because particles of $X_{AS}=0.5$, 0.6, and 0.8 behaved similarly to the $X_{AS}=0.6$ particle. During the dehydration process, the representative AS-rich particle of $X_{AS}=0.6$ exhibited a single-stage phase transition. The liquid droplet gradually decreased in size with decreasing RH and showed a phase transition at RH = 34.3–33.9%. The ERHs of all the particles are in the range of RH = 40.9–33.5%. As shown in the optical images and Raman spectra in Fig. 7, the droplet appeared to be homogeneous with the SO_4^{2-} and NO_3^- peaks at 977 and 1045 cm^{-1}, respectively, at RH = 68.8%. The droplet decreased in size abruptly at RH = 33.9%, forming a solid particle which is clearly seen by the angular shape, with the SO_4^{2-} and NO_3^- peaks shifting to 973 and 1051 cm^{-1}, respectively, indicating the droplet effloresced into the mixture of the pure AS and metastable double salt 3AN · AS (Sun *et al.*, 2019; Wang *et al.*, 2011; Ling and Chan, 2007). And the particle maintained the phase and structure with the further decrease in RH up to 6.3%.

During the humidification process, the sizes and shapes of the particles remained constant until a slight decrease in size was observed at RH = 60–68.5%, which is also seen in the optical image of the particle at RH = 66.6%. The three Raman spectra at RH = 66.6% were measured at different positions on the particle due to the seemingly heterogenous distribution when structural rearrangement occurred. As shown in the middle green-colored Raman spectrum which is for the upper part of the particle, the NO_3^- peak at RH = 66.6% showed double peaks at 1043 and 1051 cm^{-1}, indicating the transformation of a metastable 3AN·AS to a stable 2AN · AS double salt (Ling and Chan, 2007). The center and bottom parts of the particle (the orange- and blue-colored Raman spectra, respectively) seemed to be the mixture of pure AS and double salt crystals due to the pure AS crystal peak at 973 and the double peaks at 1043 and 1051 cm^{-1} shown in the corresponding Raman spectra at RH = 66.6%. All the particles absorbed water and showed a first partial deliquescence transition at RH = 68.9%, which is the DRH of the eutonic composition, i.e., MDRH of the AS-AN system in $X_{AS}>0.33$ and differed from those of $X_{AS}<0.33$. The particle became a liquid eutonic shell with a solid core structure as shown in the optical image of the particle at RH = 77.3%. Raman spectra of center and edge parts of the particle with the SO_4^{2-} peak at 973 and 977 cm^{-1}, respectively, at RH = 77.3% indicates the solid core is a pure AS crystal. Upon the further increases in RH, the particles absorbed water and grew in size until a second deliquescence transition occurred at RH = 77.8%, i.e., a second DRH, where the AS solid core dissolved completely. The particle grew continuously with the further increase in RH. The similar behavior and DRH values were observed using Raman spectroscopy in the previous study (Lee *et al.*, 2008), where the mixture exhibited one ERH around RH = 40% during the dehydration process and both solid and liquid phases of AS and only a liquid phase of AN were reported to exist between MDRH of 67% and DRH of 79%.

All other AS-rich particles of $X_{AS}>0.33$ with different mixing ratios ($X_{AS}=0.5$ and 0.8) exhibited step-wise phase transitions during the humidification process as well, i.e., the first transition at MDRH = 68.9 (±0.5)%

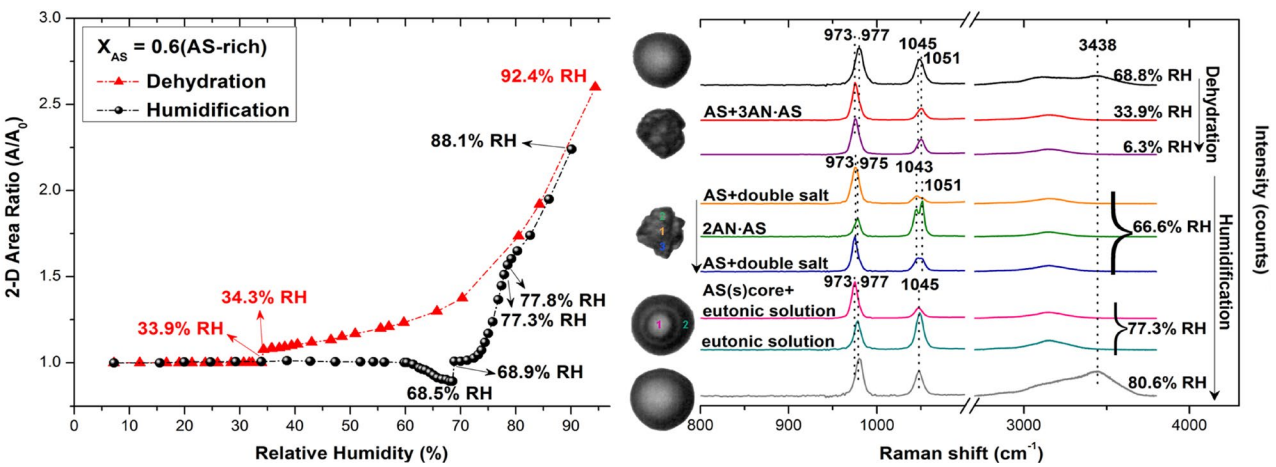

Fig. 7. Hygroscopic curve, corresponding optical images, and Raman spectra at specific RHs of an AS-rich particle ($X_{AS}=0.6$). The recorded transition RHs during the dehydration and humidification processes are marked with arrows in the hygroscopic curve.

due to the deliquescence of the eutonic component and the second one at their DRHs due to the complete deliquescence of the AS solid core. The MDRH is independent of the particle compositions, while the second DRHs are dependent on the compositions and shift toward the pure AS limit (RH = 80.7 (±0.2)%) with the increase of the AS mole fraction.

3.3 Efflorescence Phase Diagram of Mixed AS-AN Particles

Fig. 8 plots the measured ERHs for the mixed AS-AN particles as a function of the AS mole fraction. The efflorescence phase diagram is composed of two distinct phases.

1. AS(aq) + AN(aq) phase: both AS and AN are mixed in the aqueous phase above the ERHs at all mixing ratios;
2. Mixed crystal phase: RMS analysis shows that mixed droplets with various mixing ratios can crystallize into different crystal forms below the ERHs.

The observation of two phases in the efflorescence phase diagram is attributed to the one-step efflorescence of AS-AN droplets for every mixing ratio during the dehydration process. This consideration suggests core-shell structures for fully effloresced particles of AS and AN mixture, i.e., a salt with the higher mole fraction exists in the core and the outer shell has a eutonic composition. The ERH of AS-rich droplets shifted toward the pure AS limit (RH = 80.7%) when the AS content was increased. This observation supports the previous claim (Sun *et al.*, 2018), which observed the clear one-stage efflorescence at $X_{AS} > 0.3$, and the lower ERHs observed in this study compared with the previous one may be due to the different crystal formation when efflorescence occurred. The ERHs of $X_{AS} = 0.5$ and 0.6 were reported as RH = 30–27% and 32–26%, respectively, in other previous studies (Ling and Chan, 2007; Schlenker *et al.*, 2004) which are lower than those in this study. The differences can be due to the use of the collecting substrate, which might have facilitated the efflorescence in the present work (Wang *et al.*, 2017; Eom *et al.*, 2014).

3.4 Deliquescence Phase Diagram of Mixed AS-AN Particles

Fig. 9 presents the measured and theoretical MDRHs and second DRHs of the AS-AN mixture particles as a function of the AS mole fraction along with those of the

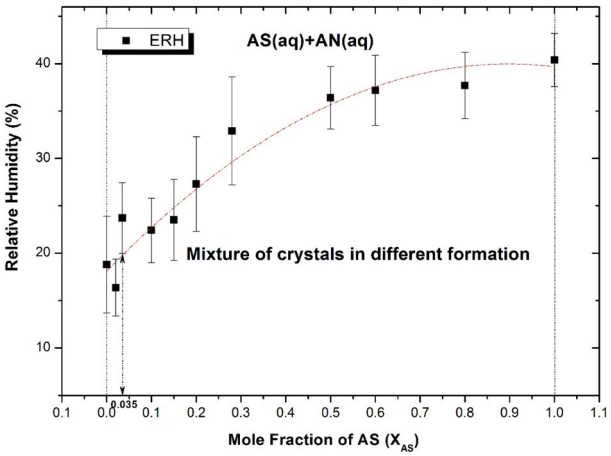

Fig. 8. Efflorescence phase diagram of AN-AS system. Measured ERH values (black bars) as a function of the mole fraction of AS in VAS-AN mixture. The phase notation shown in parenthesis is aq = aqueous. The dotted line is an imaginary boundary to show phase separation.

pure AS and AN particles. A clearly demarked phase diagram elucidating their deliquescence behavior was obtained theoretically from the E-AIM model as shown in Fig. 9, where the phase diagram of the particles within $X_{AS} = 0.15$–0.33 were shown separately due to the relatively complex situation within this range:

1. Mixture of pure AN, AS, and double salts in solid phase below the MDRH: AN(s) + 3AN·AS(s) ($0 < X_{AS} < 0.15$), AN(s) + 3AN·AS(s) + 2AN·AS(s) ($0.15 < X_{AS} < 0.2$), AN(s) + 3AN·AS(s) + 2AN·AS(s) + AS(s) ($0.2 < X_{AS} < 0.24$), 3AN·AS(s) + 2AN·AS(s) + AS(s) ($0.24 < X_{AS} < 0.33$), and 2AN·AS(s) + AS(s) ($X_{AS} > 0.33$);
2. AN(s) + AN and 3AN·AS (aq, existed in the SO_4^{2-} and NO_3^- aqueous phase) when $X_{AS} < 0.035$: a mixed phase of solid AN and aqueous eutonic components between the MDRH and second DRHs for $X_{AS} < 0.035$;
3. Mixture of pure AN, AS, and double salts (3AN·AS and 2AN·AS) both in solid and/or aqueous phases between the MDRHs and second DRHs for $X_{AS} > 0.035$;
4. AS(aq) + AN(aq) phase: both AS and AN are mixed in the aqueous phase above the final DRHs at all mixing ratios.

As shown in the theoretical phase diagram, MDRHs varied with different AS mole fractions (63.7% for 0 <

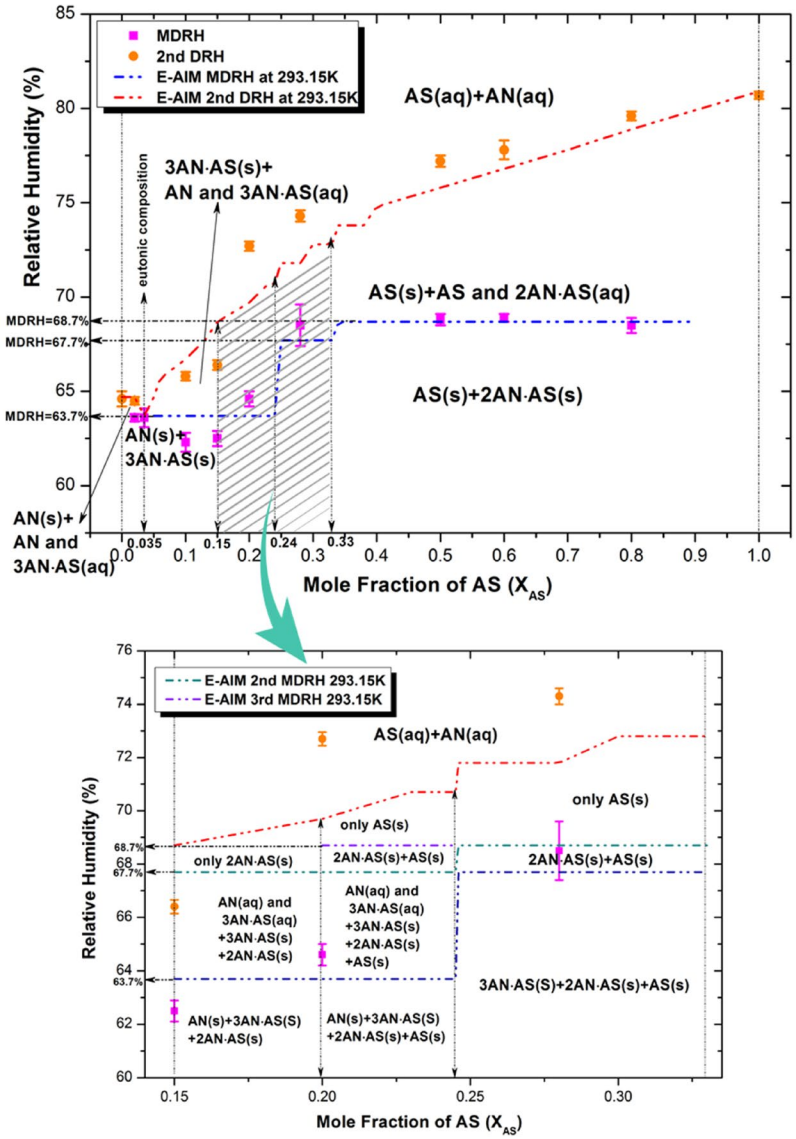

Fig. 9. Deliquescence phase diagram of AN-AS system. Measured MDRHs and second DRHs (orange and pink squares, respectively) and MDRH and second DRHs calculated from the E-AIM model (blue and red dotted lines, respectively) are plotted as a function of the mole fraction of AS in AS-AN mixture particles. The phase notations shown in parenthesis are s = solid; and aq = aqueous.

$X_{AS} < 0.24$; 67.7% for $0.24 < X_{AS} < 0.33$; and 68.7% for $X_{AS} > 0.33$), which is due to the different initial crystal formation under different mixing ratios, leading to diverse eutonic composition dissolving at their MDRHs (Fong *et al.*, 2016). The phase diagram has also been explained previously (Sun *et al.*, 2018). The experimental MDRHs of $X_{AS} = 0.02$, 0.035 (the eutonic composition), 0.5, 0.6, and 0.8, obtained in the present study, agreed well with the theoretical ones, while those of $X_{AS} = 0.1$ and 0.15 and 0.2 and 0.28 are lower and higher than the model data, respectively. Below MDRH, Raman spectra of the particles with the AS mole fractions of 0.02 and 0.035 and 0.5, 0.6, and 0.8 followed well with the predicted crystal forms (AN + 3AN · AS and AS + 2AN · AS, respectively) as shown in Figs. 3, 4, and 7, even though the AN Raman signal was not obvious in the particles of $X_{AS} = 0.02$ and 0.035 after the efflorescence, and the particles of $X_{AS} = 0.5$, 0.6, and 0.8 crystallized into the mixture of AS and 3AN · AS (Schlenker *et al.*, 2004) when the efflorescence occurred during the dehydration process before transforming into AS and 2AN · AS during the humidification process (Ling and

Chan, 2007). However, the Raman spectra of the other 4 mixing ratios did not resemble the model data, which might have led to the distinct MDRH. Fig. 9 also plots the measured second DRHs of the present work, which are lower and higher than the theoretical ones for X_{AS} = 0.1 and 0.15 and for X_{AS} = 0.2–0.8, respectively. As discussed for the particles of X_{AS} = 0.1 above, the particles of X_{AS} = 0.1 and 0.15 seemed to be somewhat in intermediate or mixing phases between the MDRH and second DRH, which may cause the lower DRH. The lower MDRHs and second DRHs of X_{AS} = 0.1 and 0.15 may be also due to the existence of a supersaturated AN moiety (Ten Brink and Veefkind, 1995). The present study also confirmed that the increase of the AN content promotes the occurrence of aqueous shell at lower RH as reported previously (Sun *et al.*, 2018). The higher second DRHs in X_{AS} = 0.2–0.8 can be due to the higher amount of AS solid core with the aqueous shell before second DRHs, which might be caused by the different metastability when the efflorescence suddenly occurred and the insufficient transformation from the metastable 3AN·AS double salt to the stable 2AN·AS double salt as the degree of the transformation is influenced by RH (Ling and Chan, 2007). Liu *et al.* (2016) also observed different DRHs between measured and calculated ones for the AS-AN mixture particles of AS:AN = 1:1 by mass due to no formation of double salts, indicating the crystal formation can be influenced by experimental conditions and other thermodynamic conditions. For the AN-rich particles (X_{AS} = 0.02), which contain more AN than the eutonic composition, the second DRH value approached the DRH of the pure AN limit as the AN concentration was increased, and for the AS-rich particles of X_{AS} = 0.2–0.8, the DRH approached that of the pure AS limit as the AS mole fraction was increased, suggesting that the second-stage deliquescence is purely driven by the remaining solid core after the deliquescence of the eutonic composition. As shown in Fig. 9, the mixture particles behaved relatively complicated in the range of $0.035 < X_{AS} < 0.33$, and some transformations inside the particles were not distinguishable by RMS analysis.

3.5 Atmospheric Implication

The knowledge of the different mixing states, the two and four distinct phases observed for the dehydration (Fig. 8) and humidification (Fig. 9) processes, respectively, and spatial distribution of chemicals in AS-AN mixture particles at various RHs have important atmospheric implications in that it is expected to help better understand the complexity of real ambient AS-AN aerosol particles, their hygroscopic properties, aqueous phase chemistry, etc. Their full efflorescence occurs at lower RHs compared with the ERH for the pure AS when AS-AN mixture droplets are formed, so that their chance for a further gas-particle interaction would be larger with less probability to fully effloresce. Even when the mixed particles become solids due to the full efflorescence below their ERHs, they can partially and fully deliquesce at lower MDRHs and DRHs, i.e., the AS-AN mixture aerosol particles can maintain an aqueous phase over a wider RH range, making their heterogeneous chemistry more probable. As described in the previous study, thermodynamic equilibrium alone cannot explain the experimental deliquescence behavior for the AS-AN mixtures and the low crystallization point of AN may cause the AS-AN particles to exist as metastable aqueous droplets at RHs lower than the MDRH (Ge *et al.*, 1998). The bigger gaps between the MDRHs and second DRHs observed in this study suggest that the particles exist as the aqueous shell with the solid core for a wider range of RH and can scatter the light more efficiently (Sun *et al.*, 2018; Adachi *et al.*, 2011). For the AS-AN mixture particles, their aqueous surface regions are crucial for atmospheric heterogeneous chemistry because the aqueous phases of AS, AN, or the eutonic composed part at different RHs are expected to be available for further reactions with gas phase species, such as N_2O_5 (Hallquist *et al.*, 2003) or organics (Wang and Laskin, 2014) to have further impacts on the atmospheric composition and air quality.

4. CONCLUSIONS

The hygroscopic behavior, physical states, and chemical micro-structures of the mixed AS-AN particles with different mixing ratios deposited on the Si wafer substrate were examined by utilizing in-situ RMS. The DRHs and ERHs of the mixed AS-AN particles in the micrometer size range at room temperature were determined by monitoring the change of the particle area in 2-D optical images and the corresponding Raman spectra at transition points with the RH variation of ~1–95%. The mixed droplets at all mixing ratios experienced single-stage efflorescence within the range of RH = 40–15%, resulting in a phase diagram consisted of two different phases. Particles with a eutonic composition of X_{AS} = 0.035 sho-

wed one-phase transition during the humidification process at MDRH = 63.6 (±0.5)%, whereas aerosol particles with other mixing ratios showed two distinct deliquescence transitions, i.e. the eutonic component dissolved first at their MDRHs, depending on their different crystal forms and then the remaining solid phase completely dissolved at various DRHs, resulting in a phase diagram consisted of four different phases. The hygroscopic properties of the atmospherically relevant AS-AN mixture particles can be crucial data for the estimation of their optical properties and direct radiative forcing. In addition, the AS-AN mixture aerosol particles can exist in an aqueous phase and/or in the form of solid core with liquid shell over a wide RH range, making their heterogeneous chemistry more significant.

DATA AVAILABILITY

The data used in this study are available upon request; please contact Chul-Un Ro (curo@inha.ac.kr).

COMPETING INTERESTS

The authors declare that they have no conflict of interest.

ACKNOWLEDGEMENT

This study was supported by Basic Science Research Programs through the National Research Foundation of Korea (NRF) funded by the Ministry of Education, Science, and Technology (NRF-2018R1A2A1A05023254) and by the National Strategic Project-Fine particle of the National Research Foundation of Korea (NRF) funded by the Ministry of Science and ICT (MSIT), the Ministry of Environment (ME), and the Ministry of Health and Welfare (MOHW) (2017M3D8A1090654).

REFERENCES

Adachi, K., Freney, E.J., Buseck, P.R. (2011) Shapes of internally mixed hygroscopic aerosol particles after deliquescence, and their effect on light scattering. Geophysical Research Letters 38, L13804, DOI: 10.1029/2011gl047540.

Ahn, K.-H., Kim, S.-M., Jung, H.-J., Lee, M.-J., Eom, H.-J., Maskey, S., Ro, C.-U. (2010) Combined use of optical and electron microscopic techniques for the measurement of hygroscopic property, chemical composition, and morphology of individual aerosol particles. Analytical Chemistry 82, 7999–8009, DOI: 10.1021/ac101432y.

Ansari, A.S., Pandis, S.N. (1999) Prediction of multicomponent inorganic atmospheric aerosol behavior. Atmospheric Environment 33, 745–757, DOI:10.1016/S1352-2310(98)00221-0.

Chan, C.K., Flagan, R.C., Seinfeld, J.H. (1992) Water activities of NH_4NO_3/$(NH_4)_2SO_4$ solutions. Atmospheric Environment. Part A. General Topics 26, 1661–1673, DOI: 10.1016/0960-1686(92)90065-S.

Chan, M.N., Chan, C.K. (2005) Mass transfer effects in hygroscopic measurements of aerosol particles. Atmospheric Chemistry and Physics 5, 2703–2712, DOI: 10.5194/acp-5-2703-2005.

Chang, S.-Y., Lee, C.-T. (2002) Applying GC-TCD to investigate the hygroscopic characteristics of mixed aerosols. Atmospheric Environment 36, 1521–1530, DOI: 10.1016/S1352-2310(01)00546-5.

Cheng, Y., Zheng, G., Wei, C., Mu, Q., Zheng, B., Wang, Z., Gao, M., Zhang, Q., He, K., Carmichael, G. (2016) Reactive nitrogen chemistry in aerosol water as a source of sulfate during haze events in China. Science Advances 2, e1601530, DOI: 10.1126/sciadv.1601530.

Ciobanu, V.G., Marcolli, C., Krieger, U.K., Zuend, A., Peter, T. (2010) Efflorescence of ammonium sulfate and coated ammonium sulfate particles: Evidence for surface nucleation. The Journal of Physical Chemistry A 114, 9486–9495, DOI: 10.1021/jp103541w.

Clegg, S.L., Brimblecombe, P., Wexler, A.S. (1998) Thermodynamic model of the system H^+- NH_4^+- SO_4^{2-}- NO_3^-- H_2O at tropospheric temperatures. The Journal of Physical Chemistry A 102, 2137–2154, DOI: 10.1021/jp973042r.

Cohen, M.D., Flagan, R.C., Seinfeld, J.H. (1987) Studies of concentrated electrolyte solutions using the electrodynamic balance. 3. Solute nucleation. Journal of Physical Chemistry 91, 4583–4590, DOI: 10.1021/j100301a031.

Cziczo, D., Abbatt, J. (2000) Infrared observations of the response of NaCl, $MgCl_2$, NH_4HSO_4, and NH_4NO_3 aerosols to changes in relative humidity from 298 to 238 K. The Journal of Physical Chemistry A 104, 2038–2047, DOI: 10.1021/jp9931408.

Denjean, C., Formenti, P., Picquet-Varrault, B., Katrib, Y., Pangui, E., Zapf, P., Doussin, J.F. (2014) A new experimental approach to study the hygroscopic and optical properties of aerosols: application to ammonium sulfate particles. Atmospheric Measurement Techniques 7, 183–197, DOI: 10.5194/amt-7-183-2014.

Dougle, P.G., Veefkind, J.P., ten Brink, H.M. (1998) Crystallisation of mixtures of ammonium nitrate, ammonium sulphate and soot. Journal of Aerosol Science 29, 375–386, DOI: 10.1016/S0021-8502(97)10003-9.

Eom, H.J., Gupta, D., Li, X., Jung, H.J., Kim, H., Ro, C.U. (2014) Influence of collecting substrates on the characterization of hygroscopic properties of inorganic aerosol particles. Analytical Chemistry 86, 2648–2656, DOI: 10.1021/ac4042075.

Fong, B.N., Kennon, J.T., Ali, H.M. (2016) Mole Ratio Dependence of the Mutual Deliquescence Relative Humidity of Aqueous Salts of Atmospheric Importance. The Journal of Physical Chemistry A 120, 3596–3601, DOI: 10.1021/acs.jpca.6b02706.

Ge, Z., Wexler, A.S., Johnston, M.V. (1996) Multicomponent aerosol crystallization. Journal of Colloid and Interface Science 183, 68–77, DOI: 10.1006/jcis.1996.0519.

Ge, Z., Wexler, A.S., Johnston, M.V. (1998) Deliquescence behavior of multicomponent aerosols. The Journal of Physical Chemistry A 102, 173–180, DOI: 10.1021/jp972396f.

Gibson, E.R., Hudson, P.K., Grassian, V.H. (2006) Physicochemical properties of nitrate aerosols: Implications for the atmosphere. The Journal of Physical Chemistry A 110, 11785–11799, DOI: 10.1021/jp063821k.

Gupta, D., Eom, H.J., Cho, H.R., Ro, C.U. (2015a) Hygroscopic behavior of NaCl-$MgCl_2$ mixture particles as nascent sea-spray aerosol surrogates and observation of efflorescence during humidification. Atmospheric Chemistry and Physics 15, 11273–11290, DOI: 10.5194/acp-15-11273-2015.

Gupta, D., Kim, H., Park, G., Li, X., Eom, H.J., Ro, C.U. (2015b) Hygroscopic properties of NaCl and $NaNO_3$ mixture particles as reacted inorganic sea-salt aerosol surrogates. Atmospheric Chemistry and Physics 15, 3379–3393, DOI: 10.5194/acp-15-3379-2015.

Gysel, M., Weingartner, E., Baltensperger, U. (2002) Hygroscopicity of aerosol particles at low temperatures. 2. Theoretical and experimental hygroscopic properties of laboratory generated aerosols. Environmental Science and Technology 36, 63–68, DOI: 10.1021/es010055g.

Hallquist, M., Stewart, D.J., Stephenson, S.K., Anthony Cox, R. (2003) Hydrolysis of N_2O_5 on sub-micron sulfate aerosols. Physical Chemistry Chemical Physics 5, 3453–3463, DOI: 10.1039/b301827j.

Haywood, J., Boucher, O. (2000) Estimates of the direct and indirect radiative forcing due to tropospheric aerosols: A review. Reviews of Geophysics 38, 513–543, DOI: 10.1029/1999rg000078.

Hoffman, R.C., Laskin, A., Finlayson-Pitts, B.J. (2004) Sodium nitrate particles: physical and chemical properties during hydration and dehydration, and implications for aged sea salt aerosols. Journal of Aerosol Science 35, 869–887, DOI: 10.1016/j.jaerosci.2004.02.003.

Hu, D., Chen, J., Ye, X., Li, L., Yang, X. (2011) Hygroscopicity and evaporation of ammonium chloride and ammonium nitrate: Relative humidity and size effects on the growth factor. Atmospheric Environment 45, 2349–2355, DOI: 10.1016/j.atmosenv.2011.02.024.

Huang, R.J., Zhang, Y., Bozzetti, C., Ho, K.F., Cao, J.J., Han, Y., Daellenbach, K.R., Slowik, J.G., Platt, S.M., Canonaco, F., Zotter, P., Wolf, R., Pieber, S.M., Bruns, E.A., Crippa, M., Ciarelli, G., Piazzalunga, A., Schwikowski, M., Abbaszade, G., Schnelle-Kreis, J., Zimmermann, R., An, Z., Szidat, S., Baltensperger, U., El Haddad, I., Prevot, A.S. (2014) High secondary aerosol contribution to particulate pollution during haze events in China. Nature 514, 218–222, DOI: 10.1038/nature13774.

Jing, B., Tong, S.R., Liu, Q.F., Li, K., Wang, W.G., Zhang, Y.H., Ge, M.F. (2016) Hygroscopic behavior of multicomponent organic aerosols and their internal mixtures with ammonium sulfate. Atmospheric Chemistry and Physics 16, 4101–4118, DOI: 10.5194/acp-16-4101-2016.

Jing, B., Wang, Z., Tan, F., Guo, Y.C., Tong, S.R., Wang, W.G., Zhang, Y.H., Ge, M.F. (2018) Hygroscopic behavior of atmospheric aerosols containing nitrate salts and water-soluble organic acids. Atmospheric Chemistry and Physics 18, 5115–5127, DOI: 10.5194/acp-18-5115-2018.

Kim, H., Lee, M.-J., Jung, H.-J., Eom, H.-J., Maskey, S., Ahn, K.-H., Ro, C.-U. (2012) Hygroscopic behavior of wet dispersed and dry deposited $NaNO_3$ particles. Atmospheric Environment 60, 68–75, DOI: 10.1016/j.atmosenv.2012.06.011.

Kim, H., Zhang, Q., Heo, J. (2018) Influence of intense secondary aerosol formation and long-range transport on aerosol chemistry and properties in the Seoul Metropolitan Area during spring time: results from KORUS-AQ. Atmospheric Chemistry and Physics 18, 7149–7168, DOI: 10.5194/acp-18-7149-2018.

Krieger, U.K., Marcolli, C., Reid, J.P. (2012) Exploring the complexity of aerosol particle properties and processes using single particle techniques. Chemical Society Reviews 41, 6631–6662, DOI: 10.1039/c2cs35082c.

Krueger, B.J., Grassian, V.H., Iedema, M.J., Cowin, J.P., Laskin, A. (2003) Probing heterogeneous chemistry of individual atmospheric particles using scanning electron microscopy and energy-dispersive X-ray analysis. Analytical Chemistry 75, 5170–5179, DOI: 10.1021/ac034455t.

Laskina, O., Morris, H.S., Grandquist, J.R., Qin, Z., Stone, E.A., Tivanski, A.V., Grassian, V.H. (2015) Size matters in the water uptake and hygroscopic growth of atmospherically relevant multicomponent aerosol particles. The Journal of Physical Chemistry A 119, 4489–4497, DOI: 10.1021/jp510268p.

Lee, A.K., Ling, T., Chan, C.K. (2008) Understanding hygroscopic growth and phase transformation of aerosols using single particle Raman spectroscopy in an electrodynamic balance. Faraday Discussions 137, 245–263, DOI: 10.1039/b704580h.

Leng, C.P., Duan, J.Y., Xu, C., Zhang, H.F., Wang, Y.F., Wang, Y.Y., Li, X., Kong, L.D., Tao, J., Zhang, R.J., Cheng, T.T., Zha, S.P., Yu, X.N. (2016) Insights into a historic severe haze event in Shanghai: synoptic situation, boundary layer and pollutants. Atmospheric Chemistry and Physics 16, 9221–9234, DOI: 10.5194/acp-16-9221-2016.

Li, X., Gupta, D., Eom, H.-J., Kim, H., Ro, C.U. (2014) Deliquescence and efflorescence behavior of individual NaCl and KCl mixture aerosol particles. Atmospheric Environment 82, 36–43, DOI: 10.1016/j.atmosenv.2013.10.011.

Li, X., Gupta, D., Lee, J., Park, G., Ro, C.U. (2017) Real-Time Investigation of Chemical Compositions and Hygroscopic Properties of Aerosols Generated from NaCl and Malonic Acid Mixture Solutions Using in Situ Raman Microspectrometry. Environmental Science and Technology 51, 263–270, DOI: 10.1021/acs.est.6b04356.

Lightstone, J.M., Onasch, T.B., Imre, D., Oatis, S. (2000) Deliquescence, efflorescence, and water activity in ammonium

nitrate and mixed ammonium nitrate/succinic acid microparticles. The Journal of Physical Chemistry A 104, 9337–9346, DOI: 10.1021/jp002137h.

Ling, T.Y., Chan, C.K. (2007) Formation and transformation of metastable double salts from the crystallization of mixed ammonium nitrate and ammonium sulfate particles. Environmental Science and Technology 41, 8077–8083, DOI: 10.1021/es071419t.

Liu, Q., Jing, B., Peng, C., Tong, S., Wang, W., Ge, M. (2016) Hygroscopicity of internally mixed multi-component aerosol particles of atmospheric relevance. Atmospheric Environment 125, 69–77, DOI: 10.1016/j.atmosenv.2015.11.003.

Liu, Y., Yang, Z., Desyaterik, Y., Gassman, P.L., Wang, H., Laskin, A. (2008) Hygroscopic behavior of substrate-deposited particles studied by micro-FT-IR spectroscopy and complementary methods of particle analysis. Analytical Chemistry 80, 633–642, DOI: 10.1021/ac701638r.

Martin, S.T. (2000) Phase transitions of aqueous atmospheric particles, Chemical Reviews 100, 3403–3454, DOI:10.1021/cr990034t.

Martin, S.T., Schlenker, J.C., Malinowski, A., Hung, H.M., Rudich, Y. (2003) Crystallization of atmospheric sulfate-nitrate-ammonium particles. Geophysical Research Letters 30(21), 2102, DOI: 10.1029/2003GL017930.

Meyer, N., Duplissy, J., Gysel, M., Metzger, A., Dommen, J., Weingartner, E., Alfarra, M., Prevot, A., Fletcher, C., Good, N. (2009) Analysis of the hygroscopic and volatile properties of ammonium sulphate seeded and unseeded SOA particles. Atmospheric Chemistry and Physics 9, 721–732, DOI: 10.5194/acp-9-721-2009.

Mikhailov, E., Vlasenko, S., Martin, S., Koop, T., Pöschl, U. (2009) Amorphous and crystalline aerosol particles interacting with water vapor: conceptual framework and experimental evidence for restructuring, phase transitions and kinetic limitations. Atmospheric Chemistry and Physics 9, 9491–9522, DOI: 10.5194/acp-9-9491-2009.

Potukuchi, S., Wexler, A.S. (1995) Identifying solid-aqueous phase transitions in atmospheric aerosols-I. Neutral-acidity solutions. Atmospheric Environment 29, 1663–1676, DOI: 10.1016/1352-2310(95)00212-H.

Schlenker, J.C., Malinowski, A., Martin, S.T., Hung, H.-M., Rudich, Y. (2004) Crystals formed at 293 k by aqueous sulfate-nitrate-ammonium-proton aerosol particles. The Journal of Physical Chemistry A 108, 9375–9383, DOI: 10.1021/jp047836z.

Schroeder, J.R., Beyer, K.D. (2016) Deliquescence Relative Humidities of Organic and Inorganic Salts Important in the Atmosphere. The Journal of Physical Chemistry A 120, 9948–9957, DOI: 10.1021/acs.jpca.6b08725.

Sun, J., Liu, L., Xu, L., Wang, Y., Wu, Z., Hu, M., Shi, Z., Li, Y., Zhang, X., Chen, J., Li, W. (2018) Key role of nitrate in phase transitions of urban particles: Implications of important reactive surfaces for secondary aerosol formation. Journal of Geophysical Research: Atmospheres 123, 1234–1243, DOI: 10.1002/2017JD027264.

Sun, Z., Duan, F., He, K., Du, J., Zhu, L. (2019) Sulfate-nitrate-ammonium as double salts in $PM_{2.5}$: Direct observations and implications for haze events. Science of the Total Environment 647, 204–209, DOI: 10.1016/j.scitotenv.2018.07.107.

Tang, I. (1976) Phase transformation and growth of aerosol particles composed of mixed salts. Journal of Aerosol Science 7, 361–371, DOI: 10.1016/0021-8502(76)90022-7.

Tang, I.N. (1996) Chemical and size effects of hygroscopic aerosols on light scattering coefficients. Journal of Geophysical Research: Atmospheres 101, 19245–19250, DOI: 10.1029/96JD03003.

Ten Brink, H., Veefkind, J. (1995) Humidity dependence of the light-scattering by ammonium nitrate. Journal of Aerosol Science, S553–S554.

ten Brink, H.M. (1998) Reactive uptake of HNO_3 and H_2SO_4 in sea-salt (NaCl) particles. Journal of Aerosol Science 29, 57–64, DOI: 10.1016/S0021-8502(97)00460-6.

Wang, B.B., Laskin, A. (2014) Reactions between water-soluble organic acids and nitrates in atmospheric aerosols: Recycling of nitric acid and formation of organic salts. Journal of Geophysical Research-Atmospheres 119, 3335–3351, DOI: 10.1002/2013jd021169.

Wang, F., Zheng, Y., Zhang, Y. (2011) Temporally and spatially resolved investigation on the efflorescence process of a mixed droplet of ammonium sulfate and ammonium nitrate. Chinese Science Bulletin 56, 2600–2603, DOI: 10.1007/s11434-011-4617-6.

Wang, J., Martin, S.T. (2007) Satellite characterization of urban aerosols: Importance of including hygroscopicity and mixing state in the retrieval algorithms. Journal of Geophysical Research: Atmospheres 112, D17203, DOI: 10.1029/2006JD008078.

Wang, X., Jing, B., Tan, F., Ma, J., Zhang, Y., Ge, M. (2017) Hygroscopic behavior and chemical composition evolution of internally mixed aerosols composed of oxalic acid and ammonium sulfate. Atmospheric Chemistry and Physics 17, 12797–12812, DOI: 10.5194/acp-17-12797-2017.

Wang, Y.Y., Jing, B., Guo, Y.C., Li, J.L., Tong, S.R., Zhang, Y.H., Ge, M.F. (2016) Water uptake of multicomponent organic mixtures and their influence on hygroscopicity of inorganic salts. Journal of Environmental Sciences 45, 156–163, DOI: 10.1016/j.jes.2016.01.013.

Wang, Z., Jing, B., Shi, X.M., Tong, S.R., Wang, W.G., Ge, M.F. (2018) Importance of water-soluble organic acid on the hygroscopicity of nitrate. Atmospheric Environment 190, 65–73, DOI: 10.1016/j.atmosenv.2018.07.010.

Wexler, A.S., Seinfeld, J.H. (1991) Second-generation inorganic aerosol model. Atmospheric Environment. Part A. General Topics 25, 2731–2748, DOI: 10.1016/0960-1686(91)90203-J.

Wexler, A.S., Clegg, S.L. (2002) Atmospheric aerosol models for systems including the ions H^+, NH_4^+, Na^+, SO_4^{2-}, NO_3^-, Cl^-, Br^-, and H_2O. Journal of Geophysical Research: Atmospheres 107, ACH 14-1-ACH 14-14, DOI: 10.1029/2001JD000451.

Wu, L., Li, X., Kim, H., Geng, H., Godoi, R.H.M., Barbosa, C.G.G., Godoi, A.F.L., Yamamoto, C.I., de Souza, R.A.F., Pöhlker, C., Andreae, M.O., Ro, C.-U. (2019) Single-particle characterization of aerosols collected at a remote site in the Amazonian rainforest and an urban site in Manaus, Brazil. Atmospheric Chemistry and Physics 19, 1221–1240, DOI:

10.5194/acp-19-1221-2019.
Yeung, M.C., Chan, C.K. (2010) Water content and phase transitions in particles of inorganic and organic species and their mixtures using micro-Raman spectroscopy. Aerosol Science and Technology 44, 269–280, DOI: 10.1080/02786820903583786.
Zawadowicz, M.A., Proud, S.R., Seppalainen, S.S., Cziczo, D.J. (2015) Hygroscopic and phase separation properties of ammonium sulfate/organics/water ternary solutions. Atmospheric Chemistry and Physics 15, 8975–8986, DOI: 10.5194/acp-15-8975-2015.
Zhang, Y., Seigneur, C., Seinfeld, J.H., Jacobson, M., Clegg, S.L., Binkowski, F.S. (2000) A comparative review of inorganic aerosol thermodynamic equilibrium modules: similarities, differences, and their likely causes. Atmospheric Environment 34, 117–137, DOI: 10.1016/S1352-2310(99)00236-8.